Influence of endohedral water on diameter sorting of single-walled carbon nanotubes by density gradient centrifugation

A. Quintillá,[a] F. Hennrich,[a] S. Lebedkin,[a] Manfred M. Kappes[abc] and Wolfgang Wenzel*[ac]

Separation of single walled carbon nanotubes (SWNT) by diameter is an important prerequisite for controlled experimental studies and efficient application of these systems. By comparing experimental data with molecular dynamics (MD) simulations, we demonstrate that water filling has a significant, tube diameter dependent effect on the effective mass density of individual single walled carbon nanotubes suspended in aqueous surfactant suspensions. We present a model for the effective density of the nanotube surfactant complex in aqueous solution that permits a comprehensive description of its density across the entire, experimentally relevant range of SWNT diameters. Parameters for this model can be obtained from molecular dynamics simulations and/or experiment and help explain the subtle interplay of surfactant coverage and endohedral water in the separation of a particular diameter species of SWNT by gradient centrifugation.

Introduction

The development and application of separation techniques for single walled carbon nanotubes (SWNTs) has become an important research field within the last few years, because present synthesis methods do not allow the growth of nanotubes of preselected length, diameter and chirality. Present date separation methods make use of liquid suspensions typically of individualized (*i.e.* debundled) tubes in water. For instance, dielectrophoretic deposition from aqueous surfactant suspensions has been used to separate metallic from semiconducting SWNTs.[1] It has more recently been shown, that separation of SWNTs by diameter can be achieved by exploiting buoyant density differences by means of ultracentrifugation of either DNA wrapped or surfactant suspended SWNTs in aqueous density gradients.[2,3]

The buoyant density of SWNTs in aqueous solution depends on multiple factors, including the mass and volume of the carbon nanotube, its surface functionalization, hydration layers and filling (if applicable). According to the simplest geometric model, which treats a nanotube as an empty hollow cylinder, the effective density of the nanotube system is expected to vary inversely with diameter. This relationship holds to lowest order independent of the complexity of the overall structure of the surfactant shell, the exterior solvent environment and other factors that are proportional to the nanotube diameter. However, such a zeroth order inverse relationship with diameter is not compatible with recent experimental work.[2] An encapsulating layer of surfactant molecules with constant thickness (Δ 2 3 nm) helps explain the observed buoyant density of the surfactant SWNT complex (1.11 1.17 g cm^{-3}) but recent work has pointed to a number of complex questions regarding the composition of surfactant solvated SWNT[4,5]

The density of SWNTs in aqueous surfactant suspensions depends on the surfactant coverage[4–7] and on SWNT hydration properties including the presence of water *inside* the tube.[8–12] Noon *et al.* found helical water sheets inside the SWNTs[13] and Brovchenko *et al.* also determined the presence of water in SWNTs.[14] Wang *et al.* performed MD simulations under ambient conditions for nanotube segments of various diameters submerged in water and inferred that single file water chains were formed in narrow nanotubes with diameters between 0.676 and 0.811 nm and that layered structures could be formed in larger diameter SWNTs.[15] Additional evidence for wetting of the inside of SWNTs and the existence of structured water layers inside the tube has been suggested by further recent molecular dynamics studies,[12] which predicted the formation of tubular water shells. Water was found to move rapidly in the hydrophobic channel formed by an SWNT.[8] However, there appears to be a minimal radius, corresponding approximately to that of the (5,5) SWNT below which water cannot penetrate the tube; minimal radii also appear to exist for more complex layered water assemblies.[15] The (outside) surface wetting of SWNTs is primarily a function of their diameter and only marginally affected by the surface details.[16]

In this investigation we investigate water filling as an additional factor influencing the observed diameter dependent variation of the effective density of solvated nanotubes. By means of MD simulations we provide: (i) a comprehensive analysis how SWNTs are suspended in water/surfactant suspensions, including the filling of tubes with water; (ii) obtain realistic estimates for the density of the water@SWNT surfactant complex; and (iii) compare these numbers with experimental findings. In this study

[a] *Forschungszentrum Karlsruhe, Institut für Nanotechnologie, D 76021 Karlsruhe, Germany. E mail: wolfgang.wenzel@kit.edu; Fax: +49 7247 826420; Tel: +49 7247 826386*
[b] *Institut für Physikalische Chemie, Universität Karlsruhe, D 76128 Karlsruhe, Germany*
[c] *DFG Zentrum für Funktionelle Nanostrukturen, Universität Karlsruhe, Wolfgang Gaede Str. 1, D 76131 Karlsruhe*

we focus on two widely used surfactants, *i.e.* sodium cholate (SCholate) and sodium dodecylsulfate (SDS).

Methods

Experimental

SWNT material was produced by the HiPco method[17] and obtained from Rice University. It was used as received. Typically ~2 mg of SWNT material were suspended in ~15 ml D_2O with 1 wt% sodium cholate (SCholate, Sigma Aldrich) using a tip sonicator (Bandelin, 200 W maximum power, 20 kHz) applied for 1 h at 10% power while cooling the sample in an ice bath. After centrifugation at 20 000 g to remove larger agglomerates, the resulting decanted suspension was then used for density gradient centrifugation (DGC) without further treatment. The DGC protocol used was similar to that described in ref. 3 except that pre formed gradients were replaced by self generated gradients (solutions of iodixanol rapidly form stable gradients under the influence of a centrifugal field). Iodixanol was purchased as OptiPrep (Sigma Aldrich) which is a 60 wt% solution in water and has a density of 1.32 g cm^{-3}. Centrifugation with an ultracentrifuge (Optima Max E, Beckman Coulter) was carried out in a fixed angle rotor (MLA 80, Beckman Coulter) at 20 °C and at 50 000 rpm for 16 20 h using Polyallomer (Bell top Quick Seal, Beckmann Coulter) centrifuge tubes. At the average radius of 45.7 mm and at the maximum radius of 61.9 mm these rotational velocities result in centripetal accelerations of 128 000 g and 173 000 g, respectively. In a typical experiment, centrifuge tubes were filled with 4 6 ml of OptiPrep to which SCholate was added to a concentration of 1 wt%. Then a layer (1 2 ml) of pure 1% surfactant solution was added. Before sealing the centrifuge tube, 1 2 ml of SWNT suspension in 1% surfactant aqueous suspension was added on top. Responding to the centripetal force during subsequent centrifugation, particles then sediment to their respective buoyant densities and spatially separate as visible stripes in the density gradient. A stable density gradient with higher density at the bottom than at the top emerges in the centrifuge tube after ~18 h. Raman measurements of iodixanol concentrations as a function of position within this gradient indicate that under typical conditions density spreads between 1.0 and *ca.* 1.4 g cm^{-3} are achievable in this fashion.

Visually, the separation of isolated SWNTs sorted by diameter/bandgap is evident by the formation of coloured bands on top of a black region which contains bundles, aggregates and insoluble material which sediment to higher density in the gradient. Fractionation was then performed as explained below. In the following, fractions with *smaller* numbers derive from regions of the centrifuge tube with *higher* density. In order to harvest the resulting fractions, we punctured small holes into the top and bottom of the centrifuge tubes and forced the liquid through the bottom hole by applying modest excess pressure through the top hole with a small syringe. The centrifuge tube contains up to 5 ml of separated materials of which roughly the topmost 1 ml contain individual tubes. Up to 50 fractions were cut in small droplets with ~25 100 μl volume (the topmost layers containing individual tubes were always fractionated in ~25 μl droplets).

The resulting fractions were than diluted to 1 ml in 1% w/v surfactant solution for optical characterization. 2D Photo luminescence (PL) contour maps of tube samples in surfactant solutions were derived from individual photoluminescence emission spectra measured in the range of 850 1750 nm with a similar setup and procedures as already described in ref. 18.

Model

In a simplified effective model, the density ρ of a water@SWNT surfactant complex (see Fig. 1) with radius r can be parameterized by the expression:

$$\rho \quad \frac{(m_{H_2O} n_{H_2O}) + \sigma_{nt} 2\pi r l + \rho_{surfactant} \pi((r+\sigma_C+\Delta)^2 \quad (r+\sigma_C)^2) l}{\pi(r+\sigma_C+\Delta)^2 l}, \tag{1}$$

where m_{H_2O} = 18 u is the mass of each water molecule in atomic mass units, n_{H_2O} the average number of water molecules inside the SWNT per unit nanotube length l, σ_{nt} is the surface density of the nanotube, $\rho_{surfactant}$ is the density of the surfactant molecules, σ_C is an effective radius of the carbon atoms and Δ is the 'thickness' of the surfactant shell around the SWNT. While the density of a particular SWNT/surfactant combination is best described by a simulation for the specific system, such a model is helpful to understand trends and parameter dependence of the behaviour of a family of SWCNT in the same solvent environment.

MD simulation

To determine the parameters n_{H_2O}, $\rho_{surfactant}$ and Δ of the model we have performed a large set of MD simulations, varying the nanotube, the water model and the surfactant. We first generated atomistic models of SWNTs of different diameters ranging from 0.5 to 1.5 nm on the basis of their chiral indices (n,m). The positions of the nanotube atoms were constrained, but the interactions between the carbon atoms and the water/surfactant molecules were taken into account. The SWNTs were solvated in a rectangular water box with periodic boundary conditions such that the edges of the box were 12 Å away from the tube. We used the OPLSAA[19] force field since it was originally parameterized for liquid simulations. We performed MD simulations in an NVT ensemble and in an NPT ensemble with the GROMACS[20,21] package. The

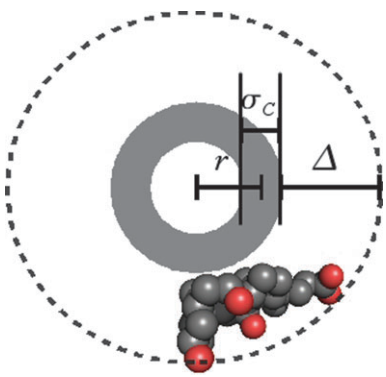

Fig. 1 Schematic representation of an SWNT cross section as surrounded by cholate molecules.

Table 1 Parameters of the LJ interaction between the carbon atoms and the water oxygen atoms. The different water models and different carbon atom parameterizations (labelled A, B and C) are represented. CA with σ 0.355 nm and ε 0.29288 kJ mol ^{1}, CB with σ 0.355 nm and ε 0.49288 kJ mol ^{1} and CC with σ 0.33 nm and ε 0.87864 kJ mol ^{1}

	SPC	TIP3P	TIP4P	TIP5P
σ_{C_AO}	0.3352 nm	0.3344 nm	0.3346 nm	0.3328 nm
ε_{C_AO}	0.4364 kJ mol ^{1}	0.4317 kJ mol ^{1}	0.4358 kJ mol ^{1}	0.4428 kJ mol ^{1}
σ_{C_BO}	0.3352 nm	0.3344 nm	0.3346 nm	0.3328 nm
ε_{C_BO}	0.5661 kJ mol ^{1}	0.5601 kJ mol ^{1}	0.5654 kJ mol ^{1}	0.5744 kJ mol ^{1}
σ_{C_CO}		0.3224 nm		0.3222 nm
ε_{C_CO}		0.7480 kJ mol ^{1}		0.7483 kJ mol ^{1}

temperature was set to 300 K and the pressure (for the simulations in the NPT ensemble) to 1 atm. Temperature coupling was achieved with a Nosé Hoover thermostat,[22] while for the pressure control, Berendsen[20] and Parrinello Rahman[23] barostats were used. To treat electrostatic inter actions, the particle mesh Ewald (PME) method was employed, while van der Waals (vdW) interactions were computed within a cut off of 14 Å. The integration time step was 2 fs for a total simulation time of 2 ns, which proved sufficient for water equilibration.

We modelled the carbon atoms as uncharged particles with a Lennard Jones (LJ) radius σ 0.355 nm and a well depth, ε 0.293 kJ mol^{-1}, corresponding to aromatic sp^2 hybridized carbon. For comparison, we performed the same calculations for different Lennard Jones parameterizations (see Table 1), but no significant differences were observed, therefore we present only the results corresponding to the parameterization specified above. The vdW diameter and well depth corresponding to the interaction potential between oxygen atoms and carbon atoms are denoted by σ_{CO} and ε_{CO}, respectively. The LJ parameters for the carbon water interactions follow the OPLSAA combination rules. As in earlier studies[8,24–26] we used σ_{CO} 0.32751 nm and ε_{CO} 0.47847 kJ mol^{-1}. For comparison Noon *et al.*[13] parameterized the LJ interactions as σ_{CO} 0.3296 nm and ε_{CO} 0.5781 kJ mol^{-1}. Wang *et al.*[15] performed MD simulations with σ_{CO} 0.3275 nm and ε_{CO} 0.4785 kJ mol^{-1} and Huang *et al.*[26] using $R_{min,CC}$ 0.1992 nm, $R_{min,OO}$ 0.17682 nm, ε_{CC} 0.0700 kJ mol^{-1} and ε_{OO} 0.1521 kJ mol^{-1}. We also analyzed how the solvent model (three point water model: SPC and TIP3P, four point water model: TIP4P and five point water model: TIP5P) affects the water behaviour inside the SWNT.

Before starting with 'production' simulations, we investigated the effects of the solvation protocol on equilibration and the dependence of equilibration time on SWNT length. Solvating the nanotube in equilibrated water at 300 K and 1 g cm^{-3} density results very long equilibration times. We thus employed a simulated annealing protocol implemented in MMTK[27] to pack the water as densely as possible inside the tube. Then, the equilibrated state is independent of the solvation protocol (see Fig. 2) after a very short simulation time (20 40 ps).

Moreover, we also analyzed the mobility of water molecules inside the tube to assure that the starting configuration had no influence on the dynamics of the system (see Fig. 3). The trajectories of individual water molecules showed that water is not trapped in the tube but is constantly exchanged with the surrounding bulk water. We thus concluded that the initial conditions did not influence the stable conformation of water inside the SWNT, therefore justifying us to proceed within this approach. After equilibration we observed the same water density for SWNTs having the same (*n*,*m*) indices for lengths between 25 Å and 200 Å. We thus chose to perform all "production simulations" with nanotubes of length 50 Å. The ends of the SWCNT were not functionalized to avoid the introduction of an end effect, since we are interested in the number of water molecules per unit length for very long tubes.

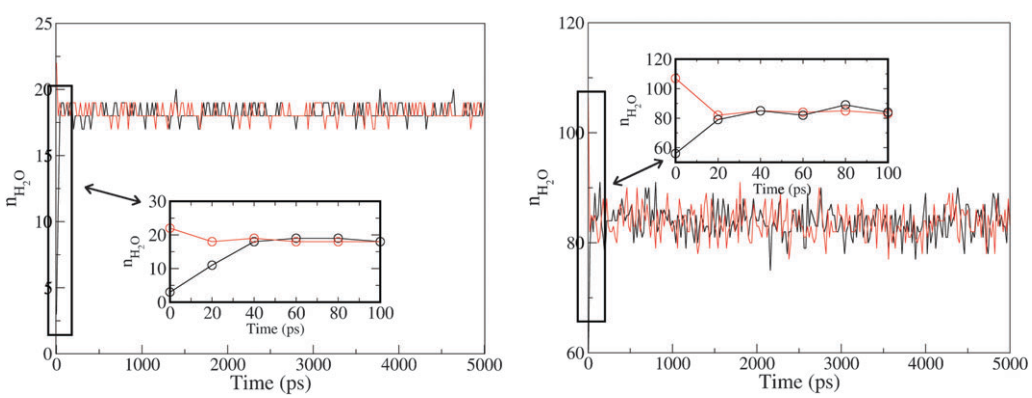

Fig. 2 Comparison of the influence of the initial configuration for SWNTs of different sizes. The number of water molecules inside the SWNT (per unit length), n_{H_2O} is plotted *vs.* the simulation time for the MMTK solvation protocol (in red) and for the standard solvation protocol (in black). n_{H_2O} is quickly stabilized after starting the simulation and remains constant for the rest of the 5 ns run. The empty nanotubes are already filled after 40 ps whereas (at the other extreme) an excess of water leaves densely filled nanotubes after 20 ps of simulation time.

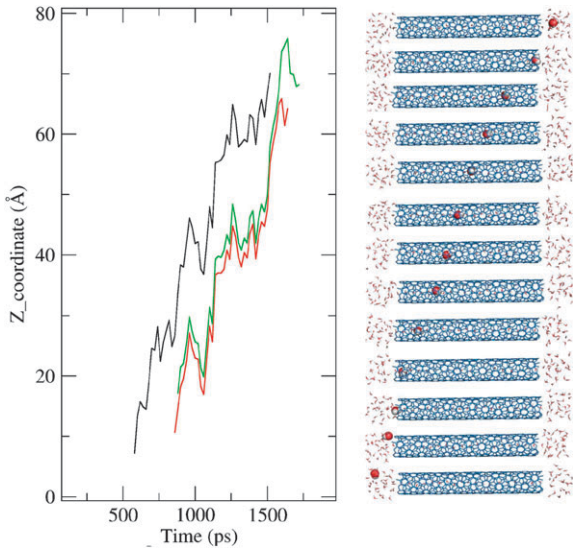

Fig. 3 Position of an individual water molecule along the tube axis as a function of time during the simulation (left panel). Snapshots corresponding to the positions of a water molecule as it moves within the tube (right panel).

Results

Photoluminescence mapping allows identifying tubes by their (*n*,*m*) chiral indices[28] and can therefore be used to study relative changes of the abundance of different (*n*,*m*) species due to sample treatment. One should keep in mind that (*n*,*m*) resolved photoluminescence intensities measured for nanotube samples do not reflect the relative abundance of specific chiral indices because: (i) metallic tubes do not photoluminesce; and (ii) associated photoluminescence cross sections for semi conducting SWNTs are predicted to be strongly dependent on chiral indices but are not accurately known.[29] Nevertheless photoluminescence maps can at least be used to compare the effects of different sample treatments for the same nanotube starting material. Fig. 4 compares photoluminescence contour maps of the starting HiPco material prior to DGC with three different fractions (fraction 10, 22 and 28) cut within the coloured bands resulting from DGC as described in the Experimental section.

From the photoluminescence contour map of the starting suspension, at least 15 different (*n*,*m*) species having diameters between 0.75 and 1.1 nm can be identified. The (*n*,*m*) distributions of fractions 10, 22 and 28 are very different from those of the starting material: (i) the DGC fraction with the highest density (fraction 10) contains mainly (9, 4), (8, 6) and (8, 4) SWNTs, with $d \sim (0.85 \pm 0.05)$ nm; (ii) the DGC fractions with slightly lower density (fraction 22 and 28) contains SWNTs with either $d < 0.8$ nm or $d > 0.9$ nm.

The experimental findings cannot be explained by a simple zeroth order inverse relationship between nanotube density and diameter. In fact one has to take into account filling of nanotubes with the water solvent as well as interactions between nanotubes and their environment.

Fig. 5 shows the number of endohedral water molecules per unit nanotube length as extracted from the MD simulations for nanotubes with diameters between 0.5 and 1.4 nm. First of all, for SWNTs with diameters below a threshold of around 0.7 nm, there are no water molecules inside the SWNT. Above this threshold single chains of water molecules are formed. For SWNTs with larger diameters (> 0.9 1.0 nm), an inner tubular water shell is formed. For the different water models studied here, we found no model dependence of the threshold diameter at which the first 'single file water channel' forms inside the SWNT. The first water channel is formed in the (6,5) CNT, which has a diameter of 0.74 nm. With increasing diameter,

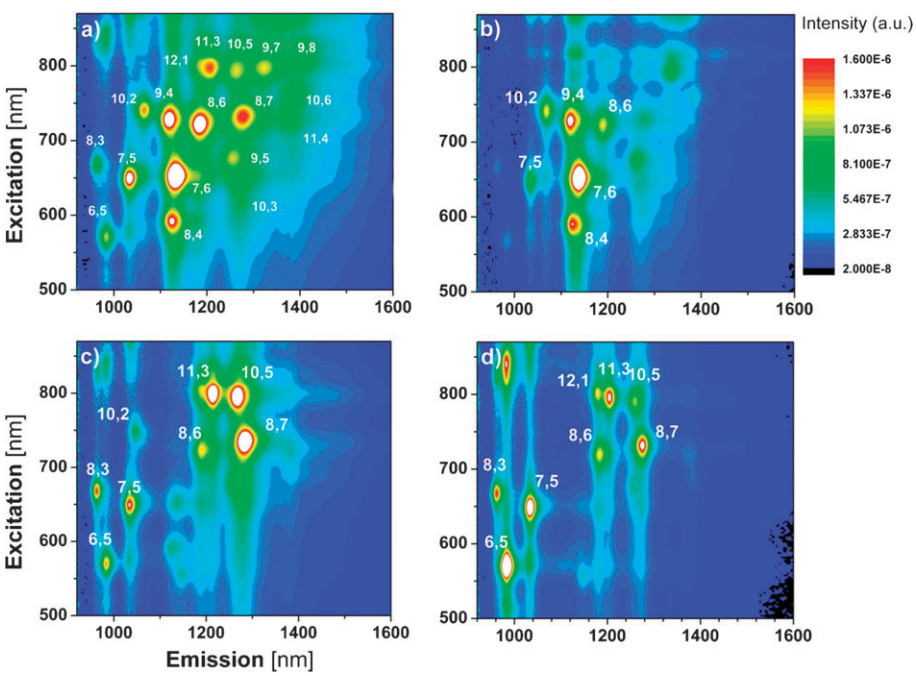

Fig. 4 Photoluminescence maps of: (a) starting HiPco SWNTs in D_2O/1% SCho and after DGC fractionation: (b) fraction 10, (c) fraction 22 and (d) fraction 28.

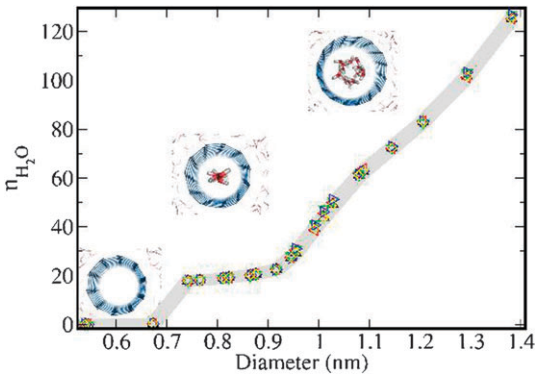

Fig. 5 Number of water molecules inside SWNTs (per unit length) *vs.* tube diameters. The different colours illustrate different pressure and temperature coupling. Also shown are snapshots of conformations corresponding to the most significant water arrangements. These indicate "single file" water filling at diameters between 0.75 and 0.95 nm, whereas larger diameter tubes show tubular water arrangements.

water molecules are able to form cylinders. Depending on the water model used, this tubular shell is already formed at 1.03 nm diameter for TIP4P and TIP5P models, whereas three point water models allow the formation of this first 'shell' only for SWNTs with larger diameters (1.15 nm). This may be due to the fact that in a five point water simulation, more polar contacts are possible, resulting in more ordered structures (closer to ice). The results of the MD simulations describe a stepwise filling of the SWNTs for a range of diameters that is not much influenced by the choice of the parameters defining the carbon atoms, nor by the water model nor by the pressure coupling algorithm. It should be noted that the simulations here were carried out in a binary system (SWNT, water), hardly realized in practice. In experiment, some effects induced by water filling may thus be broadened due to non uniform filling of the tubes.

Interaction of CNT with surfactant

Recent studies have pointed to a complexity of the morphology of the surfactant shell, after several studies that suggested deviations from a radially extending, cylindrical micelle conformation[5,30] in particular for low surfactant densities. For high surfactant density, most studies still suggest such a cylindrical model,[4,7,31] which we assumed here. We note that this assumptions becomes testable *a posteriori* by comparing the computed and experimentally observed density of the system, as discussed below.

As a proof of concept we simulated a system starting from a conformation in which surfactant molecules were diluted in water, but not attached to the SWNT. In this simulation we observed that surfactant molecules approached the tube and remained there for the duration of the simulation. Because simulations were required for every single chiral index, we performed the production simulations starting from a conformation where the surfactants are placed pointing radially outwards on the SWNT. After 2 ns of simulation, the surfactant has equilibrated, and the average number of water molecules inside the SWNT remains unchanged with respect to the SWNT solved in water. While some surfactants

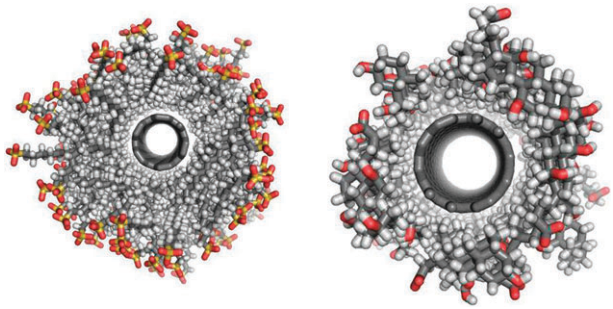

Fig. 6 Cross sections of stabilized SWNT surfactant systems for: (a) SDS and (b) cholate.

($<5\%$) diffuse away in the first few nanoseconds, the others equilibrate to positions on the tube. These surfactants stay in contact with the tube for the remainder of the 20 ns simulation indicating at least local stability of this arrangement. Starting from such conformations, we simulated the dynamics of both systems, in the NPT ensemble (at 300 K and 1 atm). The total simulation time was of 10 ns and 20 ns for each chiral index and SDS and cholate surfactants, respectively. We performed several MD simulations of a (6,5) and (10,6) SWNT in order to obtain a theoretical value for Δ and $\rho_{\text{surfactant}}$ for cholate and SDS.

In Fig. 6 we illustrate the distribution of surfactant molecules around the SWNT for an equilibrated system after 2 ns of simulation for the case of SDS and cholate. Analyzing these systems we obtain estimates of Δ_{SDS} 2.3 nm, ρ_{SDS} 1.1 g cm^{-3} and Δ_{cholate} 0.5 nm, ρ_{cholate} 1.0 g cm^{-3} for the two systems, respectively. These numbers can then be used further to calculate densities according to eqn (1) for all water@SWNT surfactant complexes investigated in this study. The presence of surfactant does not influence the water filling of the SWNT. The water behaviour inside the SWNT seems not to be influenced by the presence of surfactant in our simulations.

In Fig. 7 the density values for (water@)cholate and (water@)SDS SWNT complexes are plotted against the diameter of the tubes. We clearly observe a structured nontrivial density profile for cholate, whereas for the much larger SDS surfactant molecules, the resulting density increases monotonically with tube diameter (because here the effect of endohedral water packing on overall density is comparatively small). This correlates well with the experimental observation that (water@)cholate SWNT complexes can be separated into distinct fractions, while the (water@)SDS SWNT complexes cannot. To first order, the cholate SWNT fraction with the highest density as prepared by DGC (fraction 10; which contains mainly (9, 4), (8, 6) and (8, 4) SWNTs, corresponding to $d \sim (0.85 \pm 0.05)$ nm) can be regarded as having the same buoyant density as OptiPrep (1.32 ± 0.05) g cm^{-3}. Then qualitatively, we can rationalize the preferred fractionation of this particular SWNT diameter range as arising from its local density maximum in the corresponding water@cholate SWNT complexes. Specifically: (i) smaller diameter tubes are not filled with water and therefore have lower density; and (ii) larger tubes have decreasing density with increasing diameter until there is enough room for the

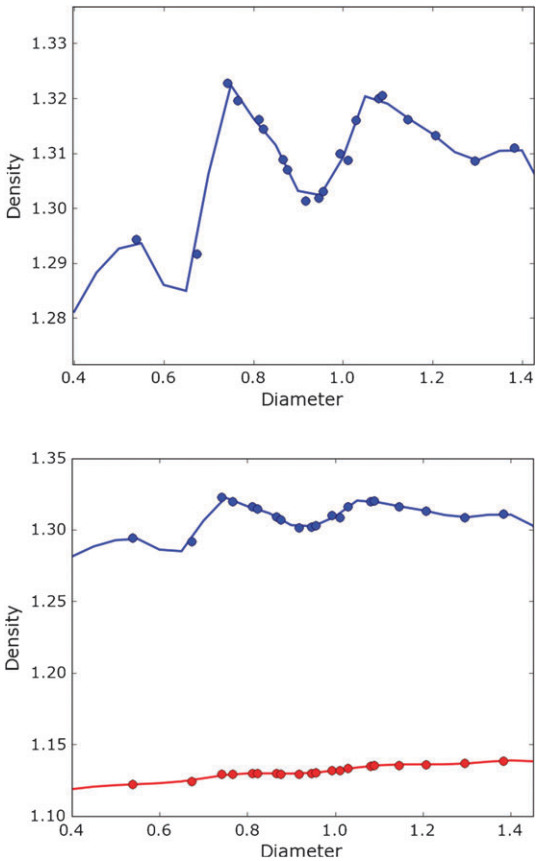

Fig. 7 Upper panel: computed densities for (water)@SWNT surfactant complexes as a function of tube diameter for cholate (blue) and SDS (red). Lower panel: expanded y axis scale representation of the cholate results.

"single file" water filling motif to be replaced by a "tubular" water arrangement. We note further, that the absolute value of the density of these systems is mainly controlled by the surfactant, which covers the largest fraction of cross sectional area of the complex. For the cholate surfactant, there is a surprisingly good agreement between the density of OptiPrep and the density calculated from MD derived estimates of the thickness and number of atoms of the cholate layer. Both of these values arise as averages of the complex configurations generated in the MD trajectories and fluctuate from snapshot to snapshot.

Our model therefore suggests that water inclusion, which is responsible for the first maximum in the density profile of the cholate SWNT complex, plays an important role in the selection of the fraction found in the centrifugation experiment. We find a peak of the density at d 0.80 nm, somewhat below the experimentally observed fraction, which contains SWNTs of diameter d 0.85 nm. When analysing the expression for the density, we find that the peak location is most strongly affected by the assumed "thickness" of the nanotubes (which enters the parameter σ_{CO}). Increasing the thickness of the SWNTs by 0.15 nm, while conserving the weight per unit length of the tube, shifts the peak to the observed experimental density. We have thus investigated possible explanations for the observed deviation between the predicted and the observed peak position. One conceivable reason could be the fact that the system is under high pressure in the experimental conditions. We have therefore performed additional simulations in the NPT ensemble with a pressure value according to the experimental conditions during centrifugation. As water is an incompressible fluid, much higher pressures do not affect its behaviour: for the system sizes we have studies the number of water molecules remains constant. The observed small dependence of water density on pressure is also an agreement with recent investigations by Yin *et al.*[32] The discrepancy between the observed peak position and the computed peak position may also be influenced by deviations of the standard interaction model between carbon and oxygen in the forcefields, which may not be quantitatively accurate for the CNT system (for which it was obviously not parameterized).

The morphology of the surfactant shell has also been widely discussed in recent investigations, following studies that suggest significant deviation from a cylindrical micelle conformation,[5,30] in particular for low surfactant densities. In our simplified model, the parameter Δ reflects the arrangement of the surfactants around the nanotube. The values extracted both from experiment and theory are compatible with a micellar arrangement of surfactants around the nanotubes, which is most pronounced for SDS. Such arrangements were also found in previous studies in the high concentration limit realized in our experimental conditions.[4,7,31] When we tune Δ towards values reflecting surfactants lying flat on the surface of the tube instead of radially pointing outwards, we cannot reproduce the observed overall density.

While our study concentrates on the role of endohedral water in the observed behaviour, it is worth noting that other mechanisms, which affect the surfactant morphology around the tube, may be important in other experimental conditions. Both tuning the electrolyte[33] or varying the surfactant density[5] may have effects that aid nanotube sorting in different centrifugation experiments.[34]

Conclusion

Separation of single walled carbon nanotubes by diameter is an important prerequisite for controlled experimental studies and efficient applications of these systems. As a result, there is presently intense activity in the SWNT separation field. Recent studies have demonstrated first separation of SWNTs according to their rollup vectors. Correspondingly, we are now at the threshold of routine SWNT electronic type and even band gap (for semiconducting SWNTs) selection. Many of the existing separation schemes employ (multiple) centrifugation steps. These could be made even more efficient by better understanding the underlying mechanisms. Back of the envelope calculations demonstrate that the diameter density dependence of the carbon nanotube alone is insufficient to lead to the observed separation of different SWNT populations according to their buoyant densities. Only secondary effects, such as water inclusion, as recently demonstrated experimentally by Homma *et al.* (private communication), or surfactant coverage could conceivably lead to successful centrifugation of a particular subpopulation.

In this study, which provides a comparison between experimental data, MD simulations and model calculations of (water@)SWNT surfactant density, we have demonstrated how the subtle interplay of surfactant coverage and endohedral water can facilitate the separation of a particular diameter species by gradient centrifugation. Our MD simulations and calculations show, that the density of the (water@)SWNT cholate complex is close to the density range of the experimentally generated gradient, whereas the (water@)SWNT SDS complex has a much smaller density. This rationalizes our observation, that under the conditions used, separation of SWNTs by buoyant density is possible for cholate but not for SDS surfactants. Furthermore, we rationalize why cholate SWNT fractions having nanotube diameters near 0.85 nm can be separated using a gradient medium having a nominal density of 1.32 g cm^{-3}. This diameter range corresponds to a local density maximum due to qualitative differences in water filling arrangements relative to both larger and smaller diameter SWNTs. Our MD simulations in fact produced a density peak somewhat below the experimentally observed fraction at 0.85 nm (see right panel of Fig. 7). Analyzing the parameters of our (water@)SWNT cholate model, we find that the peak density is most sensitive to the radius assumed in the classical carbon model for the SWNT atoms. This is not surprising, given that these parameters were taken from forcefields not parameterized for the particular carbon bonding found in carbon nanotubes. With this caveat, eqn (1) permits a comprehensive description of the (water@)SWNT surfactant density across the entire, experimentally relevant range of SWNT diameters. Our protocol also demonstrates how the parameters entering eqn (1) can be obtained from molecular dynamics simulations. This description thus permits optimization of the solvent properties to selectively target other SWNT populations.

References

1 R. Krupke, F. Hennrich, H. v. Lohneysen and M. M. Kappes, *Science*, 2003, **301**, 344 347.
2 M. S. Arnold, S. I. Stupp and M. C. Hersam, *Nano Lett*., 2005, **5**, 713.
3 M. S. Arnold, A. A. Green, J. F. Hulvat, S. I. Stupp and M. C. Hersam, *Nat. Nanotechnol*., 2006, **1**, 60.
4 M. Calvaresi, M. Dallavalle and F. Zerbetto, *Small*, 2009, **5**, 2191 2198.
5 N. R. Tummala and A. Striolo, *ACS Nano*, 2009, **3**, 595 602.
6 A. Striolo, *Nanotechnology*, 2008, **19**, 445606.
7 M. S. Arnold, J. Suntivich, S. I. Stupp and M. C. Hersam, *ACS Nano*, 2008, **2**, 2291 2300.
8 G. Hummer, J. C. Rasaiah and J. P. Noworyta, *Nature*, 2001, **414**, 188.
9 E. Dujardin, T. W. Ebbesen, A. Krishnan and M. M. J. Treacy, *Adv. Mater*., 1998, **10**, 1472 1475.
10 O. Byl, J. C. Liu, Y. Wang, W. L. Yim, J. K. Johnson and J. T. Yates, *J. Am. Chem. Soc*., 2006, **128**, 12090 12097.
11 K. Matsuda, T. Hibi, H. Kadowaki, H. Kataura and Y. Maniwa, *Phys. Rev. B: Condens. Matter Mater. Phys*., 2006, **74**, 073415.
12 N. R. d. Souza, A. I. Kolesnikov, C. J. Burnham and C. K. Loong, *J. Phys.: Condens. Matter*, 2006, **18**, S2321.
13 W. H. Noon, K. D. Ausman, R. E. Smalley and J. P. Ma, *Chem. Phys. Lett*., 2002, **355**, 445.
14 I. Brovchenko, A. Geiger and A. Oleinikova, *Eur. Phys. J. B*, 2005, **44**, 345 358.
15 J. Wang, Y. Zhu, J. Zhou and X. H. Lu, *Phys. Chem. Chem. Phys*., 2004, **6**, 829.
16 M. P. Rossi, H. Ye, Y. Gogotsi, S. Babu, P. Ndungu and J. C. Bradley, *Nano Lett*., 2004, **4**, 989 993.
17 M. J. Bronikowski, P. A. Willis, D. T. Colbert, K. A. Smith and S. R. E., *J. Vac. Sci. Technol., A*, 2001, **19**, 1800.
18 S. Lebedkin, K. Arnold, F. Hennrich, R. Krupke, B. Renker and M. M. Kappes, *New J. Phys*., 2003, **5**, 140.
19 W. L. Jorgensen and N. A. McDonald, *J. Mol. Struct*., 1998, **424**, 145 155.
20 H. J. C. Berendsen, D. Van Der Spoel and R. Van Drunen, *Comput. Phys. Commun*., 1995, **91**, 43.
21 D. Van Der Spoel, E. Lindahl, B. Hess, G. Groenhof, A. E. Mark and H. J. C. Berendsen, *J. Comput. Chem*., 2005, **26**, 1701.
22 D. J. Evans and B. L. Holian, *J. Chem. Phys*., 1985, **83**, 4069 4074.
23 M. Parinello and A. Rahman, *J. Appl. Phys*., 1981, **52**, 7182 7190.
24 K. Wang, B. Fain, M. Levitt and R. Samudrala, *BMC Struct. Biol*., 2004, **4**, 8.
25 T. Werder, J. Walther, R. Jaffe, T. Halicioglu and P. Koumoutsakos, *J. Phys. Chem*., 2003, **B107**, 1345 1352.
26 B. Huang, Y. Xia, M. Zhao, F. Li, X. Liu, Y. Li and C. Song, *J. Chem. Phys*., 2005, **122**, 084708.
27 K. Hinsen, *J. Comput. Chem*., 2000, **21**, 79 85.
28 S. M. Bachilo, M. S. Strano, C. Kittrell, R. H. Hauge, R. E. Smalley and R. B. Weisman, *Science*, 2002, **298**, 2361 2366.
29 S. Reich, C. Thomsen and J. Robertson, *Phys. Rev. Lett*., 2005, **95**, 077402.
30 K. Yurekli, C. A. Mitchell and R. Krishnamoorti, *J. Am. Chem. Soc*., 2004, **126**, 9902.
31 E. J. Wallace and M. S. P. Sansom, *Nano Lett*., 2007, **7**, 1923.
32 B. Yin and S. L. Dong, *Chin. Phys. Lett*., 2009, **26**.
33 S. Niyogi, C. G. Densmore and S. K. Doorn, *J. Am. Chem. Soc*., 2009, **131**, 1144.
34 N. Nair, W. J. Kim, R. D. Braatz and M. S. Strano, *Langmuir*, 2008, **24**, 1790.